

Channel Characteristics and User Body Effects in an Outdoor Urban Scenario at 15 and 28 GHz

Kun Zhao, Carl Gustafson, *Member, IEEE*, Qingbi Liao, Shuai Zhang, Thomas Bolin,
Zhinong Ying, *Senior Member, IEEE*, and Sailing He, *Fellow, IEEE*

Abstract—The effect of a user’s body on channel characteristics for single user downlink transmission in an urban scenario for the fifth generation (5G) systems is investigated with ray-tracing at 15 and 28 GHz. Three different designs of user equipment (UE) antennas are fabricated and integrated into a mobile phone prototype, and their 3-D radiation patterns are measured both with and without a user. The user remains in Cellular Telephone Industries Association (CTIA) standard data mode and talk mode during measurements. The results show that the user’s body will cause a strong shadowing loss and generate a large fluctuation on the received signal strength of the UE at both 15 and 28 GHz, which is crucial to channel modeling studies at frequencies above 6 GHz. In addition, the user’s body effect on a linear array system in an UE is presented, and the main challenges for the future work are also addressed.

Index Terms—5G, array, body effect, channel, millimeter wave (mmWave), mobile phone, user equipment (UE).

I. INTRODUCTION

THE demands for high-speed wireless communications are ever increasing. However, the data rate and spectral efficiency of current 4G/LTE cellular systems are limited by the relatively small amount of bandwidth and the number of antennas that are being used. One attractive method to improve the spectral efficiency of the next generation wireless systems operating below 6 GHz is to employ a massive number of antennas at the base station (BS). These so-called Massive MIMO systems can utilize spatial multiplexing to serve multiple users simultaneously using the same time-frequency resources [1], [2]. In order to further resolve the issue of spectrum shortage and improve peak data rates, frequency bands above 6 GHz and into the millimeter wave (mmWave) range above 30 GHz have also been identified as attractive candidates for future 5G cellular system. This is

Manuscript received December 29, 2016; revised July 24, 2017; accepted August 2, 2017. Date of publication August 17, 2017; date of current version November 30, 2017. This work was supported by Swedish VR under Grant 621-2011-4620. (*Corresponding author: Kun Zhao*.)

K. Zhao, Q. Liao, and S. He are with the School of Electrical Engineering, Royal Institute of Technology, 10044 Stockholm, Sweden (e-mail: kunzhao@kth.se).

C. Gustafson is with Department of Electrical and Information Technology, Lund University, 22100 Lund, Sweden.

T. Bolin and Z. Ying are with the Network Technology Laboratory, Sony Mobile Communications AB, 22188 Lund, Sweden.

S. Zhang is with the Department of Electronic Systems, Antennas, Propagation and Radio Networking Section, Aalborg University, 9220 Aalborg, Denmark.

Color versions of one or more of the figures in this paper are available online at <http://ieeexplore.ieee.org>.

Digital Object Identifier 10.1109/TAP.2017.2740959

motivated by the large contiguous frequency bands that these higher frequencies can offer [3]. Recently, the Federal Communications Commission announced that 3.85 GHz of licensed spectrum is being opened at frequencies above 24 GHz, and 14 GHz of unlicensed spectrum will be allocated between 57 and 71 GHz [4]. A downside of millimeter frequencies is, however, that as the carrier frequency increases, propagation conditions become less favorable. For antennas with a fixed antenna gain, the received power in free space decreases with the square of the carrier frequency, and is therefore much smaller compared to sub-6 GHz frequency bands. Conversely, if the physical antenna aperture size remains fixed at both the transmitter (Tx) and the receiver (Rx), the received power in free space increases with the square of the carrier frequency. Therefore, the additional free space path loss at higher mmWave frequencies can be mitigated or overcome with adaptive antenna array systems and beamforming techniques. In addition to this, the penetration and diffraction losses at mmWave frequency bands will also be more severe than in current cellular bands [5]–[7]. Furthermore, human bodies and other blocking objects can cause sharp shadow zones in higher frequency bands as their dimension increases in terms of wavelengths [8]–[10]. Therefore, many challenges still need to be solved in order to fulfill the targeted demands of 5G communication.

Research on centimeter and mmWave communication systems has been carried out since the late 80s for outdoor communications [5], [11]. During the 2000s, the unlicensed 60 GHz band attracted a lot of interest, mainly for indoor Wi-Fi scenarios, where human blockage and severe penetration losses were identified as major challenges [9], [12], [13]. In more recent years, the research focus from both industry and academia has been geared toward 5G outdoor communications for both cellular and fixed systems. Several studies for the outdoor scenario have been carried out, which have resulted in a number of path loss models that have been proposed for the frequency bands at 28, 38, 60, and 73 GHz [14]–[24]. Extensive ray-tracing results at 28 GHz in an urban environment have also shown that the path loss can exhibit different behaviors along different streets [20] and that the large-scale shadow fading variance of the overall path loss increases with distance [21]. These effects need to be considered to preserve spatial consistency.

In order to combat large path loss and severe shadowing, cellular systems above 6 GHz will rely on beamforming to ensure a sufficient link budget. The received power is

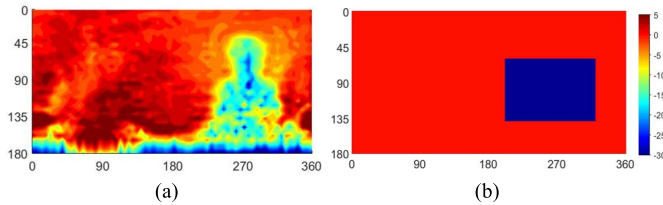


Fig. 1. User shadowing gain patterns based on (a) measurement with a real user in CTIA data mode at 15 GHz and (b) 3GPP self-blocking model in portrait mode.

highly impacted by the instantaneous beamforming patterns of antenna arrays at the Tx and the Rx [25]. Ideally, a channel model should include both large-scale and small-scale features of the channel, as well as the impact of arbitrary array configurations and antenna elements. Antenna radiation pattern requirements are provided in the 3GPP TR 38.901 channel model for frequencies from 0.5 to 100 GHz [26]. However, the cellular channels can also be drastically impacted by the user's body, as it directly impacts the user equipment (UE) antenna efficiency and radiation pattern. Therefore, the actual radiation patterns (possibly with beamforming), especially for the UE antennas together with the user's body, should also be included to obtain a channel model that resembles the real situation more closely. In cellular bands below 6 GHz, previous studies have mainly focused on the efficiency loss of antennas with a user body [27]–[29]. However, with increased frequency, a more pronounced shadowing loss on the radiation of the UE antenna will become the dominant effect [30], [31]. So far, some studies have been performed regarding human blockage in mmWave bands for indoor [9], [12], [13] and outdoor scenarios [32], [33]. The 3GPP TR 38.901 [26] model also supports two different blockage models: A and B. Model B is a geometric model based on diffraction around screens, and is useful for describing deterministic shadowing occurring at a far-field distance from the antennas. Model A is a stochastic model, based on blocking regions, including one self-blocking region due to the user. The attenuation of each cluster within this self-blocking region is 30 dB, and 0 dB outside this region. The studies above and the 3GPP standard are, however, based on simplified blockage models. The user body effect on the UE antenna in real life will be more complicated: the interaction between UE antennas and the user can happen in both the near field and the far-field of the antenna, as the way that users hold their phone can vary dramatically in real life. The blockage regions from a real user can also be different when compared with the standard models. Fig. 1 shows a comparison of the measured shadowing gain due to a real user in CTIA data mode at 15 GHz with the 3GPP self-blocking model in portrait mode for frequencies above 6 GHz. The measured shadowing gain is determined based on the difference between the measured far-field pattern with and without the user. The measurement settings will be explained in detail in Section III.

Ray-tracing is a popular tool to obtain the deterministic site-specific channel models, and it has been successfully used for modeling wireless channels [34]–[37]. In this paper, we evaluate the user body effect on the channel characteristics

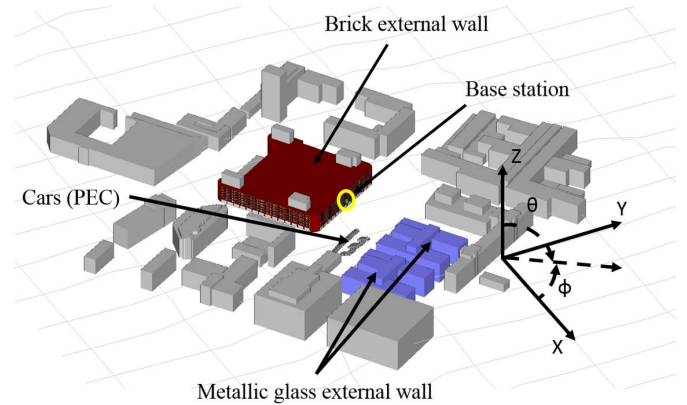


Fig. 2. 3-D model of the study area in ray-tracing simulations.

of the downlink for a single user case at 15 and 28 GHz using ray-tracing. At 15 GHz, the results from the ray-tracer are compared with measurement-based results performed at Ericsson using their 15 GHz 5G test bed [38]. We also present ray-tracing results at 28 GHz, as this band has been identified by the ITU as one of the main candidate 5G carrier frequencies [39]. Furthermore, three different antenna designs for the UE have been fabricated at 15 and 28 GHz, respectively. These antennas are integrated into a mobile phone prototype and have radiation patterns and polarizations that are complementary to each other, which provides a good basis for the comparison. The user body effect on the UE antennas is investigated through measurements of the 3-D antenna radiation pattern: the antennas are measured with and without the user's presence, where the user holds the phone as defined by the CTIA data mode and talk mode. The measured antenna patterns are added to the ray-tracing simulation results to determine their impact on the channel characteristics.

The paper is organized into four parts as follows. The accuracy of the ray-tracing simulations is first verified with the Ericsson 5G test bed measurement results in Section II. The human body effect is discussed in Section III, with also considering the randomness of the UE orientation. Effects of implementing a linear array in the UE in both data and talk mode are discussed in Section IV. Finally, we summarize the main results of this paper and identify the main challenges for future works in the conclusion. The ray-tracing simulations in this paper are carried out by Wireless Insite (v.2.8), and the measurements at 15 and 28 GHz are conducted in the Microwave Vision Group Lab in Paris, France, and at Aalborg University in Aalborg, Denmark.

II. VERIFICATION OF RAY-TRACING SIMULATION IN URBAN SCENARIOS

We have performed ray-tracing simulations of an outdoor urban area in Kista, Stockholm, Sweden. The area is mainly occupied by 4–6 office buildings with heights around 15–20 m, as shown in Fig. 2. The total area of study is about 500 m × 550 m. θ and ϕ represent the elevation and azimuth angles, respectively. The ray-tracing simulation is carried out using the commercial software Wireless

TABLE I
SIMULATION SETUP FOR RAY-TRACING VERIFICATION

Parameter	Value
Reflection	6
Diffraction	1
Transmission	0
TX height [m]	8.5
RX height [m]	2.9
Minimum Path Gain [dB]	-190
Frequency [GHz]	15
Bandwidth [MHz]	200
Noise Floor [dBm]	-75

Insite (v.2.8) for the 3-D propagation environment [40]. The simulation settings are summarized in Table I. The number of reflections, diffractions, and transmissions are set to obtain an accurate simulation while keeping the computational complexity reasonably low. The small numbers of diffractions and transmissions are mainly due to their limited effect in such high-frequency bands [36]. In our simulations, no dramatic change can be observed by further increasing these numbers. A minimum path gain of -190 dB is chosen to match the dynamic range that is typically achieved in channel measurements today [17]. The choice of this minimum path gain value is further motivated by the fact that the results remain virtually unchanged when using an even lower minimum value.

The physical environment of the study area is modeled by a detailed 3-D map that includes, among other things, buildings, windows, and parked cars. A measurement campaign at 15 GHz was conducted by Ericsson using their 5G test bed in the same location [38]. The positions of the BS and UE antennas are chosen based on the measurement campaign: the BS plays as the Tx, hanging on the external wall of the red brick building and 8.5 m above the ground. In the measurement, the UE (as Rx) is installed on the top of a van, which is 2.9 m above the ground. The van was driven within the study area at speeds of 0–30 km/h during the measurement. In the simulation, the structure and the speed of the van is ignored for simplicity. In the simulation model, more detailed structures are added to the red brick building and the twin buildings behind the parking lot, since they are closer to the Tx. The external walls of the red and the blue buildings are modeled as brick and metallic glass, respectively. The structures of the windows and the window frames are also included for these two buildings. Several cars are placed in a parking lot with PEC material. The rest of the buildings in the study area are modeled as concrete for simplicity, and the terrain is modeled as wet ground. The permittivity of the materials used in this simulation at 15 and 28 GHz is listed in Table II, where the values are mainly determined by ITU recommendations [41], [42].

For verification, the ray-tracing simulation results at 15 GHz are compared with measurement results from the Ericsson 5G test bed. The details of the measurement can be found in [38]. In the measurement, the received signal strength of a 4×4 MIMO system is measured through two 100 MHz carriers, which are aggregated into a total of 200 MHz

TABLE II
MATERIAL PERMITTIVITY

Material	Real part of relative permittivity	Conductivity S/m
Frequency [GHz]	15 / 28	15 / 28
Concrete	5.31	0.29 / 0.48
Brick	3.75	0.038
Glass	6.27	0.11 / 0.23
Metallic Glass	6.27	15
Wood	5	0
Wet Ground	10 / 6	4 / 9
Metal	PEC	PEC

bandwidth centered at 15 GHz. The 4×4 MIMO system is composed of two vertically polarized antennas and two horizontally polarized antennas. The transmitting power of each Tx is 30 dBm. Each Tx antenna has a peak gain of 15 dBi, an azimuth half power beamwidth (HPBW) of 90° , and an elevation HPBW of 8.6° . The Rx antenna element has roughly omnidirectional characteristics in the horizontal plane with a 1 dBi peak gain. The comparisons between the simulated and measured received signal strengths are presented in Fig. 3. The Rx in the measurement has a noise floor of -75 dBm, which has also been added to the simulation results in this section in order to recover the measurement results.

The simulated received signal strength of each Rx position is obtained through the channel transfer function: the transfer function and received power between Tx antenna m and Rx antenna n in the simulation is obtained by the following equations:

$$H_{m,n}(k) = \sum_{l=1}^L (g_{r,n}^V(\vartheta_l^{rx}) g_{r,n}^H(\vartheta_l^{rx})) \begin{pmatrix} a_{l,m,n}^{VV} & a_{l,m,n}^{VH} \\ a_{l,m,n}^{HV} & a_{l,m,n}^{HH} \end{pmatrix} \begin{pmatrix} g_{t,m}^V(\vartheta_l^{tx}) \\ g_{t,m}^H(\vartheta_l^{tx}) \end{pmatrix} e^{-i2\pi \Delta f \tau_l k} \quad (1)$$

$$P_{rx} = \sum_{k=1}^K \frac{P_{tx}}{K} * |H_{m,n}(k)|^2 \quad (2)$$

where $g_{r,n}^V(\vartheta_l^{rx})$, $g_{r,n}^H(\vartheta_l^{rx})$, $g_{t,m}^V(\vartheta_l^{tx})$ and $g_{t,m}^H(\vartheta_l^{tx})$ are the vertical (V) or horizontal (H) components of the complex antenna gain at angle of departure ϑ_l^{rx} and angle of arrival (AoA) ϑ_l^{tx} . L and K are the total numbers of plane waves and sub frequencies, where l and k are the subindices of the plane wavenumber and frequency. Δf is the ratio between the total bandwidth and $K-1$. a_l and τ_l are the complex amplitude and time delay of the plane wave l , respectively.

The simulated and measured received signal strength of the UE within the study area is presented in Fig. 3(a), and the received signal strength as a function of the distance between the BS and the UE is plotted in Fig. 3(b). It can be observed that the simulated data agree well with the measurements at different locations. The difference between the simulated and the measured signal strength is shown in Fig. 3(c) for a street canyon route and a corner route [as marked in Fig. 3(a)].

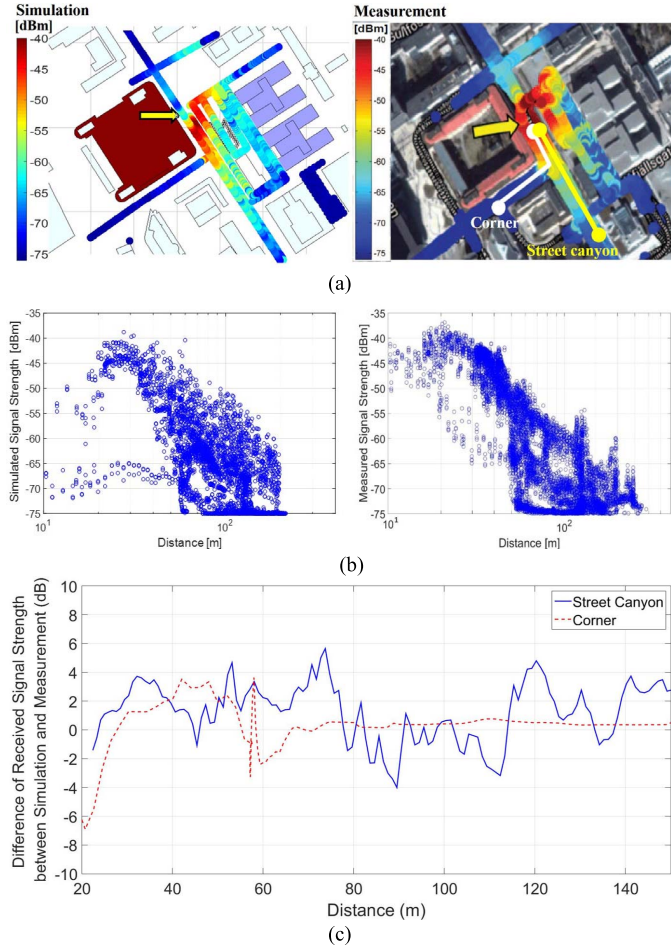


Fig. 3. Comparison between simulation and measurement results of (a) received signal strength overview, (b) received signal strength versus distance, and (c) difference between simulated and measured signal strength in street canyon and corner scenarios [(a) is reproduced from [27] with permission].

The root mean square logarithm error of the simulation is 2.5 dB on the canyon route, which shows that the simulation results agree well with the measurement results. (The deviation in the corner scenario becomes negligible when the distance is above 80 m as the signal strength drops to the noise floor.) Therefore, it can be concluded that the simulation model is accurate enough to evaluate the overall channel characteristics. It is worthy to mention that the simulations were not performed using the exact same locations as the user as in the measurements, and that we cannot obtain a perfect fit due to the inaccuracies of the measured global positioning system positions. It is therefore not possible to attain perfect agreement with the measurements.

As the measurement system is limited to 15 GHz, it is impossible to compare the simulation and measurement results at 28 GHz. However, the major difference between the 15 and 28 GHz channel is mostly attributed to the different wavelengths. Considering the materials in the study area are mainly nondispersive or only weakly dispersive between 15 and 28 GHz, the propagation paths at 28 GHz are expected to be similar to those at 15 GHz. Therefore, the simulation model at 28 GHz can also give a good estimate of the received signal strength.

TABLE III
SIMULATION SETUP FOR RAY-TRACING WITH
INTEGRATED PHONE ANTENNA

Parameter	Value
Reflection	6
Diffraction	1
Transmission	0
TX antenna	Omni-directional
RX antenna	Integrated UE antenna
TX height [m]	8.5
RX height [m]	1.6
Minimum Path Gain [dB]	-190
Frequency [GHz]	15/28
Bandwidth [MHz]	200
Noise Floor [dBm]	NA
Tx Power [dBm]	30

III. USER BODY EFFECT ON THE CHANNEL CHARACTERISTICS

The channel characteristics with measured radiation patterns of the 5G phone prototype with and without user effects are presented in this section. In order to evaluate the user body effect on the channel characteristics, the measured UE antenna radiation patterns with and without a user are implied into the ray-tracing simulated channel models. The analysis in this section will be based on a single antenna in the UE in order to focus on the fundamental properties of the user body effect.

The simulation setup of the propagation channel in ray tracer is listed in Table III. The major part of the simulation is the same as in Section II, as the simulation model has been verified to be accurate in predicting the channel characteristics. However, no noise is included in the ray-tracing simulations in Sections III and IV in order to obtain the exact path loss at each position. Moreover, since we focus on the impact from the UE in this study, the BS antenna is modeled as a single omnidirectional antenna. If 32 antennas were used at the base station for each sector, the array gain would be close to 15 dB. In order to simplify the calculations, we instead add a 15 dB array gain directly to the received power in the simulation results in Sections III and IV, which allows us to focus more on the properties of the user body effect. The total transmitted power is assumed to be 30 dBm, with both polarizations having equal power. The bandwidth of the simulations at 15 and 28 GHz is chosen to be 200 MHz, and the height of the BS is 8.5 m, which are the same as in the simulation in Section II. The height of the UE antenna is lowered to 1.6 m in order to mimic a real-life scenario.

Three antenna designs for the UE are investigated in this paper: 1) a notch antenna; 2) a slot antenna; and 3) an edge-patch antenna. The proposed antennas are realized at both 15 and 28 GHz with the same designs (same antenna types and feeding methods) but in different dimensions in order to become resonant at 15 and 28 GHz, respectively. The physical dimensions of the proposed antenna elements are approximately 6 mm × 1 mm at 15 GHz and 4 mm × 0.8 mm at 28 GHz. The dimensions are slightly different between each design in order to optimize the antenna impedance matching.

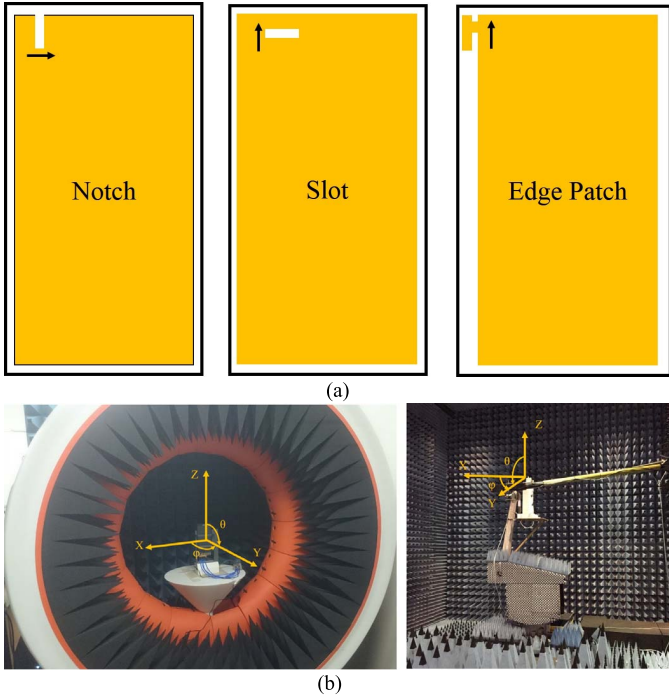


Fig. 4. (a) Schematic and the polarizations of proposed antennas in the phone prototype and (b) measurement setup at 15 and 28 GHz.

All proposed antennas are placed at the top of the phone, as shown in Fig. 4(a), and their radiation patterns and polarizations are complementary to each other in order to provide a good basis for comparison. The details of the antenna design and their spatial coverage efficiencies can be found in [30] and [31]. The corresponding measurement setups in free space at 15 and 28 GHz are presented in Fig. 4(b), and the measured radiation patterns are plotted in Fig. 5. The edge patch radiates in opposite directions at 15 and 28 GHz, as the antennas were installed on left and right sides of the phone prototype, respectively. It is worthwhile to mention that the measurements were carried out using different measurement systems due to the different frequency bands. For the measurements at 28 GHz, the radiation patterns are only measured from 0° to 140° in elevation angle due to the mechanical limitations of the system. However, since most of the plane waves arrive at the UE side from the elevation angles $\theta < 120^\circ$ in the ray-tracing simulations, this issue will not impact the results dramatically.

A. UE Without User Body Obstruction

The simulated received signal strength and the outdoor coverage area with the integrated notch, slot, and edge-patch antenna in a mobile phone prototype as the UE are presented in Fig. 6. The phone is placed vertically relative to the ground plane, and the display faces toward the direction of azimuth angle $\phi = 120^\circ$ of the study area (correspond to the coordinate system in Fig. 2). Only the edge patch at 28 GHz is rotated 180° in order to make it radiate in the same direction as in the 15 GHz simulation. Though the radiation patterns of the three UE antennas point in different directions and their

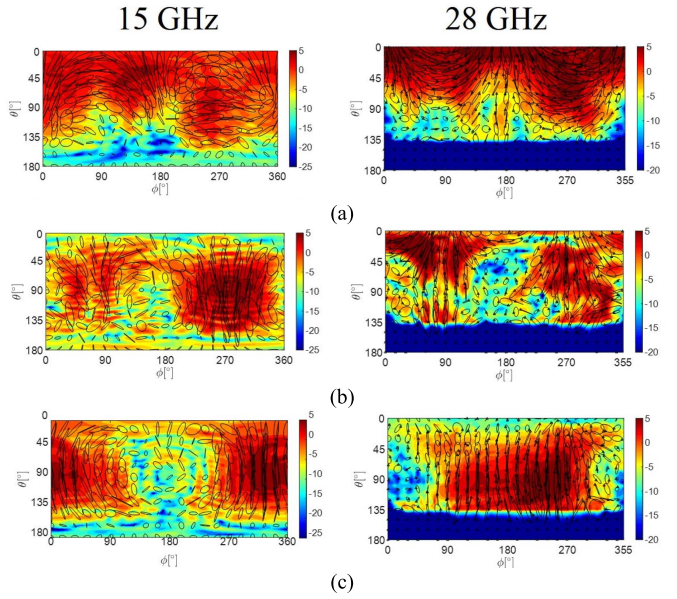


Fig. 5. Measured radiation patterns of (a) notch antenna, (b) slot antenna, and (c) edge-patch antenna in a phone prototype at 15 and 28 GHz without user body obstruction.

polarizations are complementary with each other, it can be observed that the received signal strength of the UE in different locations and the overall coverage of the BS with three different antenna designs are very similar: within the study area, the received signal strength is typically above -60 dBm in the line-of-sight (LOS) region, but below -80 dBm in the non-line-of-sight (NLOS) regions with all three UE antenna designs. Therefore, the specific UE antenna design may not be the most critical factor to extend the coverage of 5G systems above 6 GHz.

It can also be observed that the larger free space path loss (5.4 dB) at 28 GHz leads to a slightly worse coverage compared to 15 GHz in the LOS and the LOS-NLOS transition regions. However, regardless of the antenna type or the operation frequency, the proposed communication system is difficult to cover the NLOS region, where the received signal strength drops dramatically compared to the LOS regions due to the building blockage. For instance, the received signal strength in the region behind of the twin metallic glass buildings is around 40–50 dB lower than the signal strength on the main street with the same Tx-Rx separation distance.

B. UE With User Body Obstruction

For UE antennas, only discussing the performance in the absence of a human user is not enough; the corresponding antenna performance and channel characterization has to be evaluated with a user body present. In our study, two user holding cases are considered: data mode and talk mode. These user holding cases can be found in the CTIA over-the-air (OTA) standard [43]. Standard body phantoms are widely used for the OTA performance evaluation of mobile phones below 6 GHz, but it has not been extended to the frequency band above 6 GHz yet. Therefore, we measured the antenna performance with real users in this study.

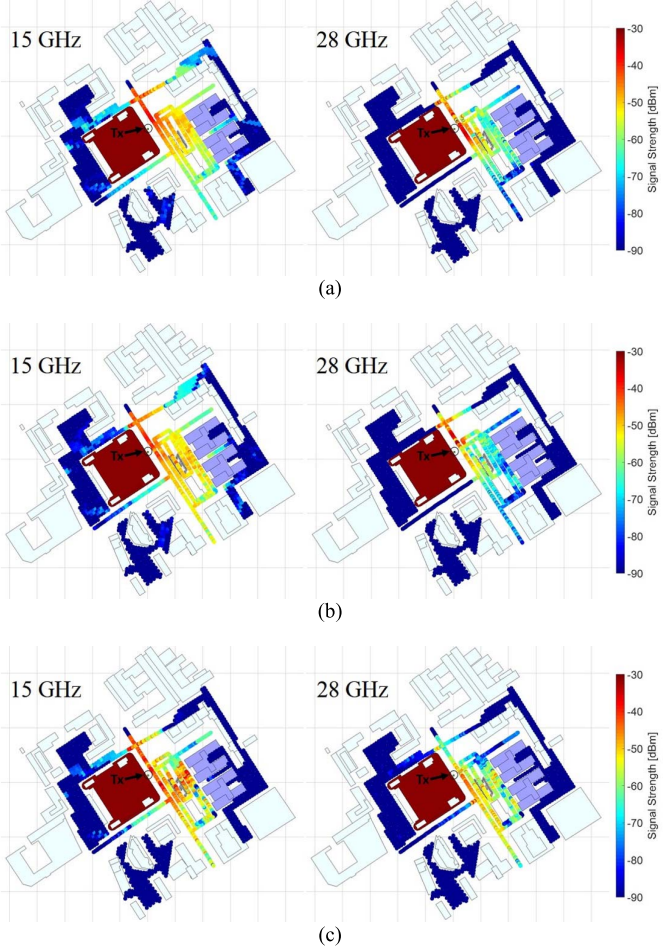


Fig. 6. Coverage overview with (a) notch antenna, (b) slot antenna, and (c) edge patch antenna in the UE without user body obstruction.

The corresponding measurement setup is presented in Fig. 7 and radiation patterns are plotted in Fig. 8. With the user present, the antenna pattern is no longer best described by only the antenna element itself, but rather as a super antenna [44] that includes both the integrated antenna element and the user. During measurements, the user remained in static positions based on the CTIA standard data and talk modes. The UE is held 30 cm away from the user's torso in data mode. It also should be noted that the measurements at 15 GHz are carried out with the same user, but the measurements at 28 GHz are measured with three different users due to its much longer measurement time (around 15 min at 28 GHz and only 5 min at 15 GHz).

As the measurements at 15 and 28 GHz are carried out on the left- and the right-hand sides, respectively, the radiation patterns in talk mode at 15 and 28 GHz are opposite to each other. Therefore, a deep shadowing region caused by the user's head in talk mode can be observed at $\phi = 0^\circ$ at 15 GHz, but at $\phi = 180^\circ$ at 28 GHz. A low antenna gain region can also be observed at $\phi = 180^\circ$ in data mode at 28 GHz, but not at 15 GHz, which is due to a narrower beamwidth of the antenna radiation pattern at higher frequencies. This low gain region can also be observed in measurement results without the user body obstruction at $\phi = 0^\circ$ at 28 GHz (Fig. 5).

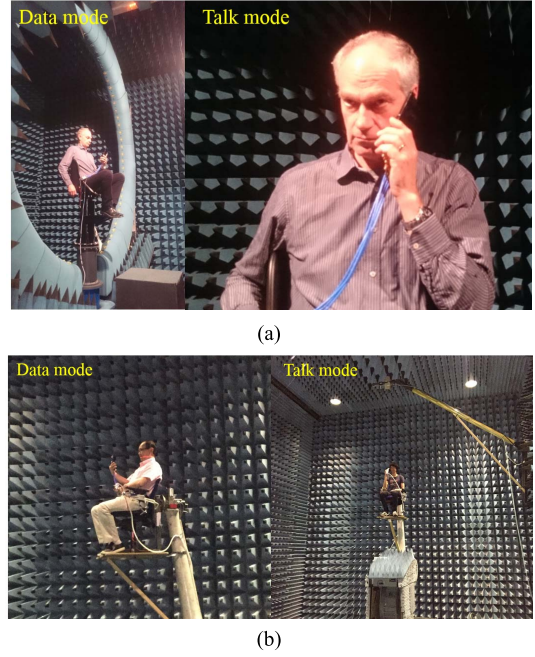


Fig. 7. Measurement setup of the user holding cases at (a) 15 and (b) 28 GHz.

TABLE IV
TOTAL EFFICIENCY OF THE PROPOSED ANTENNAS

Frequency (GHz)	Notch		Slot		Edge Patch	
	15	28	15	28	15	28
Without User (dB)	-0.2	-0.4	-1	-1.4	-0.5	-0.2
Data mode (dB)	-0.5	-3.4	-2.5	-4.8	-2	-2.8
Talk mode (dB)	-2	-3.5	-3.5	-6.9	-2.2	-5

The user body effect on UE antennas can be categorized into three aspects: 1) the impedance mismatching; 2) the radiation power absorption; and 3) the shadowing effect. In the cellular bands below 6 GHz, effects on the impedance mismatching and the power absorption are major concerns, since the user body mainly appears in the reactive near field of the antenna. At 15 and 28 GHz, the user body effect on the antenna impedance mismatching and the radiation power absorption is expected to be lower compared to the frequency bands below 6 GHz, as the distance between the user body and the UE antenna is much larger in terms of wavelengths. This can be verified by the measurement results of total efficiencies in Table IV: the total efficiency loss is only about 2 dB in data mode and 3–4 dB in talk mode, which is much lower than their counterparts below 6 GHz (e.g., typically 6–10 dB in talk mode). The total efficiency is defined as the ratio of the total radiated power to the total input power of the antenna, and the total efficiency loss includes antenna conductive loss, dielectric loss, mismatching loss and the mutual coupling loss.

On the other hand, the shadowing effect of the user body becomes much more severe, and a clear body-shaped shadowing zone can be observed in the data mode at both frequency points. The deepest shadowing loss in the horizontal plane ($\theta = 90^\circ$) is about 25 dB in data mode and 30 dB in talk

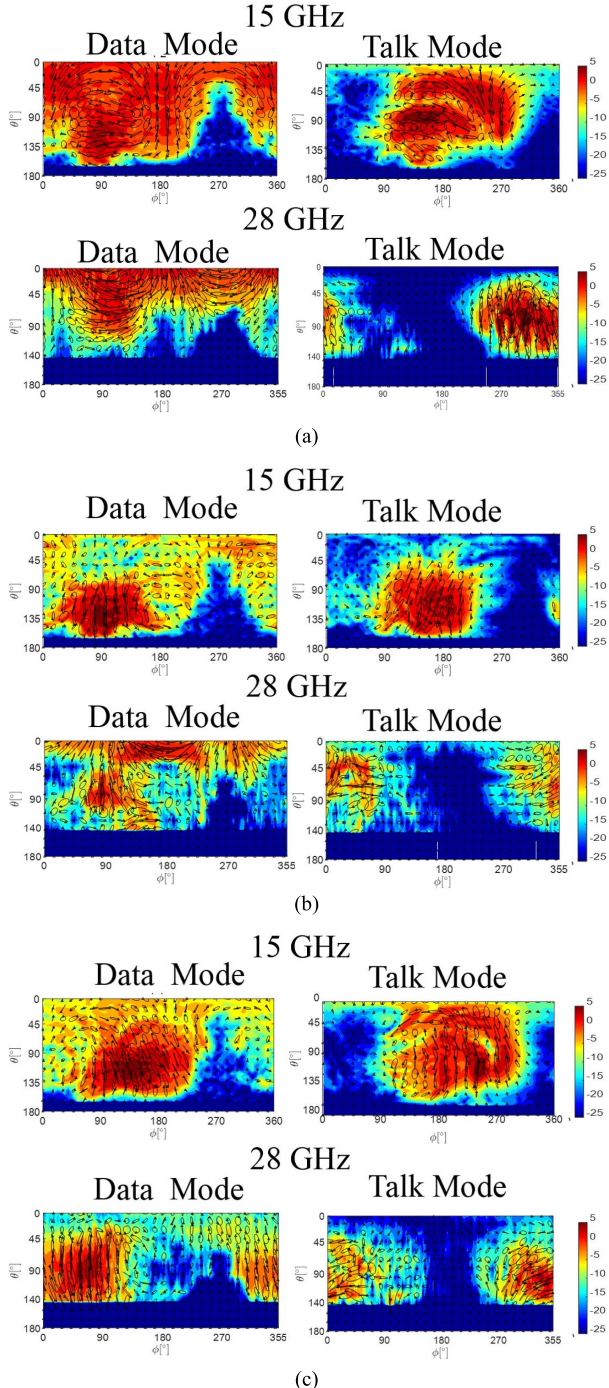


Fig. 8. Measured radiation patterns of (a) notch antenna, (b) slot antenna, and (c) edge-patch antenna in a phone prototype at 15 and 28 GHz with real users.

mode at 15 GHz. Meanwhile, the shadowing loss at 28 GHz is about 5 dB higher than at 15 GHz in both modes. These values are comparable with the self-blocking loss of 30 dB as defined in the 3GPP model [26], but the observed shadowing regions are different from the 3GPP model, as previously shown in Fig. 1. It has also been reported in [31] that the variation of the shadowing loss can be up to 4 dB with different users in talk mode. It is therefore expected that the shadowing loss will vary between different users as well as between different

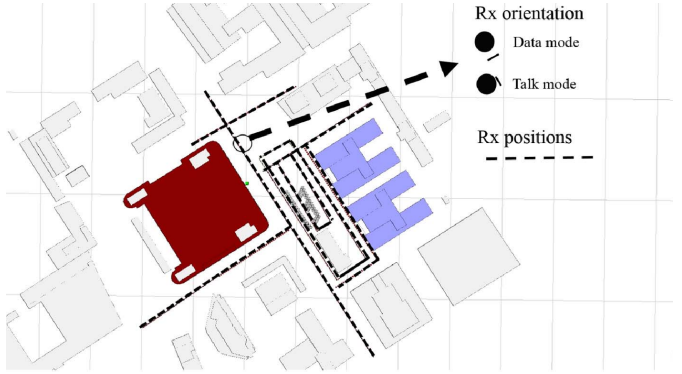


Fig. 9. Simulated Rx positions and the relative orientation of the user and the UE in data and talk mode.

frequency bands in real life. More measurement results of the body effect on the UE antennas at 15 and 28 GHz can be found in [30] and [31].

The analysis in the free space scenario has shown that the proposed system has poor coverage in some deep NLOS areas. Therefore, these areas are excluded from the analysis in this section in order to emphasize the user body effect on the received signal strength. In the first step, we examine the channel characteristics with the fixed orientations of the UE and the user. The simulated Rx positions are placed along routes in LOS areas that shown as dashed lines in Fig. 9. The relative orientations of the user and the UE in the data and talk modes are also illustrated, which remain the same in all positions. The radiation patterns at 28 GHz are rotated 180° to make sure their relative positions of the BS, the user, and the UE are the same as in the 15 GHz scenario. The corresponding received signal strength of the UE and the coverage overview are presented in Figs. 10–13.

From Figs. 10 and 11, it can be observed that coverage of the BS are very similar between different antenna designs in the same user holding case at 15 and 28 GHz. However, the differences in coverages with different user holding cases are very large, and the effect of user body blockage on the coverage area can be clearly observed. The reason for this phenomenon is that effective radiation patterns of the three antennas become similar when the user holds them in the same way. Moreover, by comparing the received signal strength against distance for the three proposed antenna designs in Figs. 12 and 13, it can be observed that slopes of signal strengths are very similar between different antenna elements in the same user holding case, but quite different for different user holding cases. For example, the path loss exponents (PLE) in data mode with the notch, the slot, and the edge patch antenna at 15 GHz are -3.4 , -3.3 , and -2.9 , respectively. On the other hand, the PLE in talk mode of the notch antenna at 15 GHz is only -1 , which is sharply different to the value in data mode.

It can also be observed that the coverage area of the system at 28 GHz in Fig. 11 is slightly smaller than at 15 GHz in Fig. 10 due to the extra path loss and higher shadowing loss from the user body. From Figs. 12 and 13, the received signal strength without user obstruction at 28 GHz is on average 5 dB

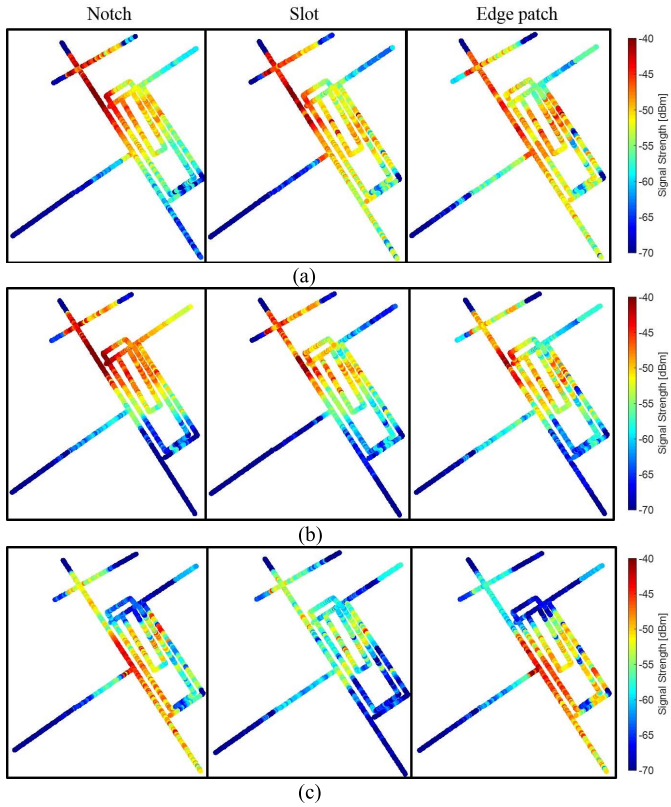


Fig. 10. Coverage overview (a) without user body obstruction, (b) in data mode, and (c) in talk mode at 15 GHz.

lower compared to at 15 GHz, due to the smaller antenna apertures. However, the received signal strength at 28 GHz in data mode and talk mode is on average 10 dB lower than at 15 GHz, where the extra 5 dB loss is mainly caused by a more pronounced user body effect at a higher frequency.

In talk mode, the received signal strength is dramatically reduced when the user moves closer to the BS for all three antenna designs. The reason for this peculiar phenomenon is that the number of multipath components is reduced when the user moves closer to the BS, and a strong LOS signal becomes the dominant component in transmission. However, with this certain orientation of the user and UE in Fig. 9, the user's head will block this dominant LOS component in talk mode, and the only viable signal paths are reflected from buildings or objects that are opposite to the BS. The reflected signals travel much further than the LOS path, which leads to a drop in the received signal strength when the user is very close to the BS in talk mode.

Based on the above observations, it can be concluded that for the downlink transmission in the single user scenario, the impact of the individual antenna design in the UE is not as important as the user effect when determining system-level performance, the BS coverage, and a channel model.

C. UE With User Body Obstruction With Random Orientation

In reality, the orientation of the UE and the user is random. As we have observed that the user body effect can have a

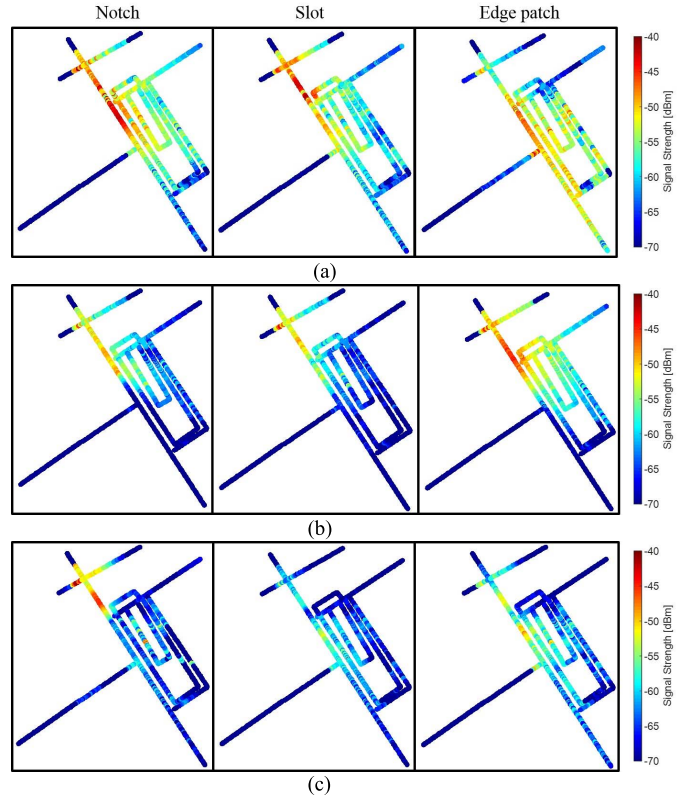
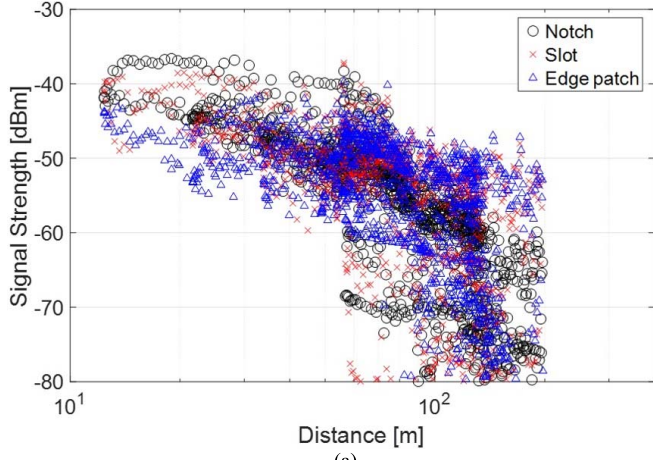


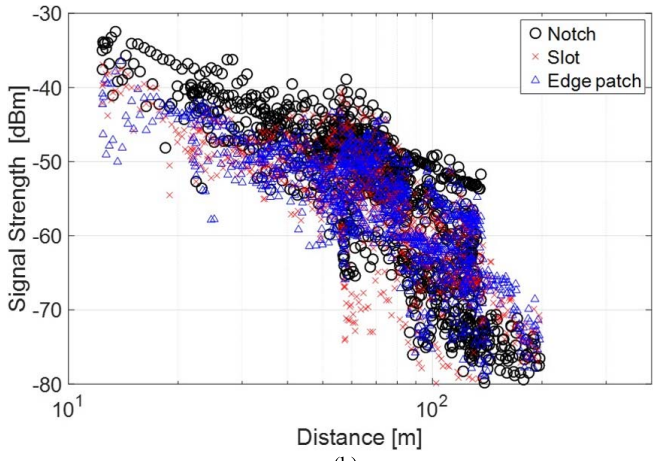
Fig. 11. Coverage overview (a) without user body obstruction, (b) in data mode, and (c) in talk mode at 28 GHz.

dramatic impact on the received signal strength, the statistical performance of the received signal has to be evaluated considering the randomness of the orientation of the UE and the user. Therefore, the effective radiation patterns of the UE antenna without user's presence (Fig. 5), in data mode, and in talk mode (Fig. 8) are rotated in the horizontal plane from 0° to 360° (in 10° step) in different locations to provide a further understanding of the user body effect on the channel characteristics.

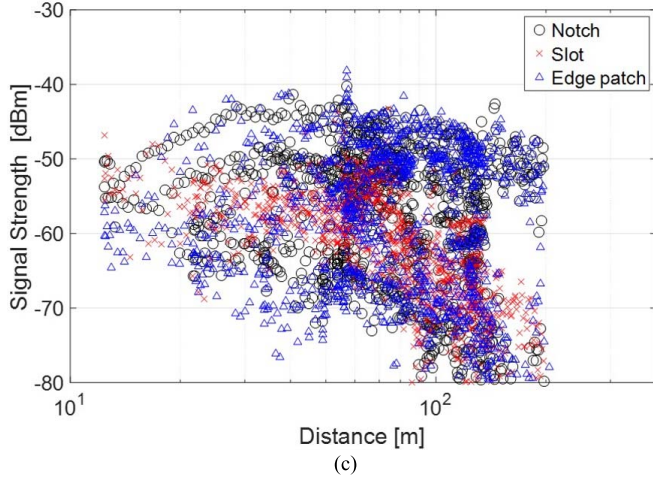
The received signal strength for each rotation angle is recorded, which enables us to evaluate the corresponding empirical distribution and the variation of received signal strength. Since we have concluded that the impact of different antenna designs on the channel characteristics is less important than the user body effect, only the notch antenna is examined here. The reason is that the notch antenna shows the best omnidirectional pattern in the horizontal plane when the user is absent (as shown in Fig. 5), which is usually desired for the UE and can show the user body effect more clearly. The UE and the user rotation are carried out in three routes with three typical scenarios in the urban environment, as shown in Fig. 14. They are referred to as the urban canyon scenario, the corner scenario, and the parking lot scenario. In the urban canyon and the corner scenario, the AoA spread is relatively narrow. However, in the parking lot scenario with cars, the AoA spreads more uniform over the horizontal plane. Moreover, the corner scenario also includes a LOS to NLOS transition region. The three scenarios can cover the effect from



(a)



(b)

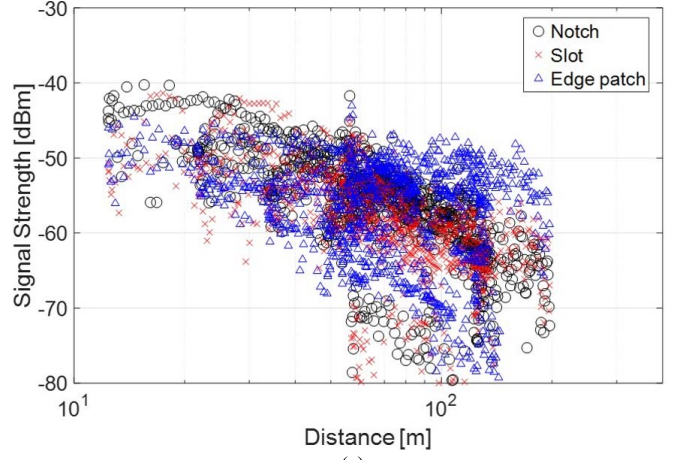


(c)

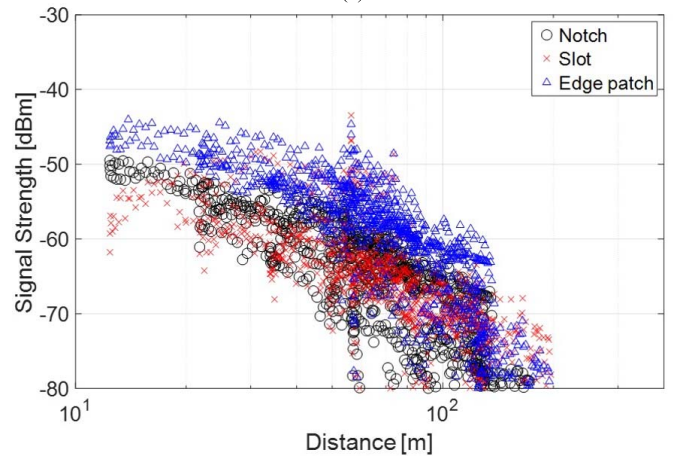
Fig. 12. Received signal strength (a) without user body obstruction, (b) in data mode, and (c) in talk mode at 15 GHz.

a rich scattering environment, a poor scattering environment, and the waveguide effect in a street canyon, which can provide a good understanding of user body blocking effects under different propagation conditions.

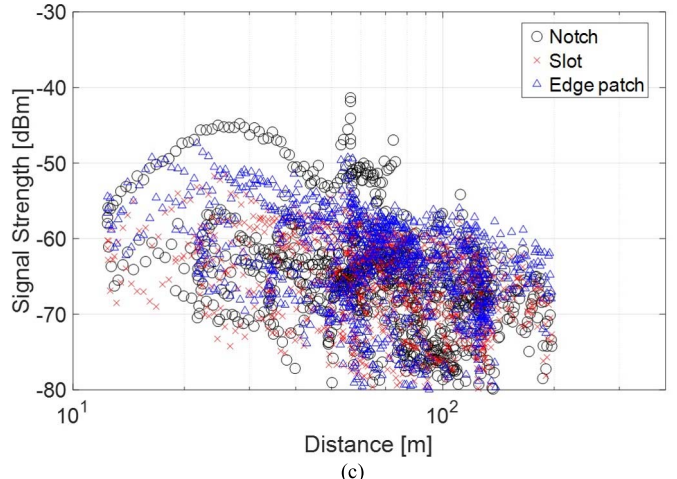
The empirical probability density functions (PDF) of the received signal strengths for the integrated notch UE antenna at 15 GHz with arbitrary rotation angles are plotted in Fig. 15, and the corresponding average values and standard deviations (SDs) are given in Table V. In the urban canyon



(a)



(b)



(c)

Fig. 13. Received signal strength (a) without user body obstruction, (b) in data mode, and (c) in talk mode at 28 GHz.

scenario, we can observe that the SD of the received signal is dramatically increased when the user presents in the urban canyon scenario. This phenomenon is caused by the increased directional radiation pattern of the super antenna (includes both the UE antenna and the user) due to the interaction between the UE antenna and the user body, as well as the small angular spread due to the waveguide effect of the street canyon. Moreover, the talk mode also exhibits a larger variance

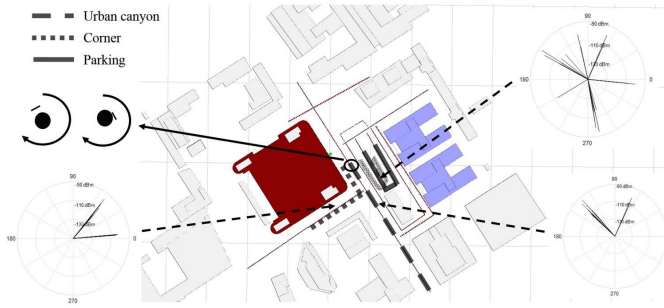


Fig. 14. Rx positions and AoA in the urban canyon, the corner, and the parking lot scenarios.

TABLE V
MEAN AND STANDARD DEVIATION OF THE SIGNAL STRENGTH SAMPLING DISTRIBUTIONS FOR WITH ROTATED UE ORIENTATION

Scenario	User case	15 GHz	28 GHz
		Mean [dBm]/SD [dB]	Mean [dBm]/SD [dB]
Urban Canyon	Without user	-52.2/5.8	-62.5/5.5
	Data mode	-52.7/7.3	-62.7/7.3
	Talk mode	-55.3/10.2	-64.1/10.9
Corner	Without user	-54.5/9.7	-65.4/9.9
	Data mode	-55.2/10.7	-66.5/11.9
	Talk mode	-58.2/13.3	-66.7/14.0
Parking	Without user	-48.4/3.3	-59.3/3.3
	Data mode	-48.3/3.2	-59.5/5.0
	Talk mode	-49.2/5.4	-56.5/5.5

with a more pronounced tail probability compared to the data mode, as the UE is more close to the user body. Similar conclusions can be drawn regarding the corner scenario, but it is worthwhile to note that there is an 18 dB corner loss at 15 GHz and that the variation of received signal strength also increases after turning around the corner due to the lack of an LOS component and waveguide effect from the street canyon. However, the distribution of the received signal in the parking lot area is much more concentrated with and without the user's presence, and its SDs are also clearly smaller than in the urban canyon and corner scenarios. It can be observed from Fig. 14 that the AoA in the parking region is distributed more uniformly in the horizontal plane due to its rich scattering environment, which reduces the variation of the received signal strength, making it less sensitive to user orientation.

The absolute variation of the received signal strength against distance at 15 GHz is also presented by its mean, minimum, and maximum values with rotated user and UE orientations in Fig. 15. It can be seen that the mean values with and without the user are quite similar (with a difference of less than 5 dB) in all three propagation scenarios. This is mainly due to the negligible total efficiency loss in the data mode and the talk mode. The maximum value in talk mode is about 1–2 dB higher than the other two cases as the antenna peak gain is increased, since the user's head acts as a reflector. However, due to the strong variation of the minimum signal strength with and without the user, the dynamic range of the signal strength is clearly enlarged in the urban canyon and corner

scenarios. In the urban canyon scenario, the absolute variation of signal strengths in talk mode can be up to 36 dB when the UE is 190 m away from the BS, which is 18 dB larger than the case without the user.

Additionally, the variation of received signal strength in the urban canyon scenario also tends to increase with increasing Tx–Rx separation distance, where the absolute variation of the signal strength is enlarged from 20 to 36 dB with the UE moved from 20 to 190 m away from the BS in talk mode. This phenomenon is likely due to reduced angular spreads along the street canyon. Similar results were observed in [21], but without considering the user body effect. This means that, in general, channels in such a high frequency will exhibit a variance that is increasing with distance, and the user body effect can increase this effect further. It is also worth noting that the received signal strength is increased when the UE is getting close to the BS in talk mode, which appears to be the opposite of what is observed in Figs. 12(c) and 13(c). However, this is because the values here are obtained from multiple orientations instead of a fixed orientation, and the minimum distance between the UE and the BS here is also not small enough to observe this phenomenon.

The shape of the sampling distribution of the received signal strength at 28 GHz is similar to the results obtained at 15 GHz. The mean values and SDs are also given in Table V. The average received signal strength at 28 GHz is 10 dB lower than at 15 GHz, but the SD is similar to the 15 GHz case. From the results above, we can see that, even in the LOS region, the received signal strength can suffer from huge fluctuations due to the random orientations in different user holding cases if the angular spread is narrow, since the angular spread for reception of the UE antenna is dramatically reduced due to the shadowing effect of the user's body. This phenomenon cannot be avoided through single antenna optimizations. The fluctuation of the received signal strength for different orientations is also strongly related to the relative distance between the UE and the user body, where in talk mode, the variation of received signal strength is about 5–10 dB larger than in the data mode. Unless properly addressed, this phenomenon could cause severe issues with coverage even in a typical urban canyon scenario.

IV. IMPACT OF UE ARRAY CONFIGURATION

From the previous section, we can conclude that cellular systems operating at 15 and 28 GHz with a single antenna on the UE side cannot yield sufficient coverage in the NLOS region. Furthermore, in both the LOS and NLOS scenarios, the received signal will sometimes degrade dramatically due to severe shadowing caused by the user's body. One possible solution for the above issues is to implement antenna arrays with beamforming capabilities on the UE side. This idea was already proposed during early discussions on mmWave cellular systems [45]. However, the performance of beamforming arrays integrated into the UE with a user body effect present has not yet been investigated. In this section, the received signal strength of an 8×1 linear array and a single antenna in the phone prototype are compared for two user holding cases.

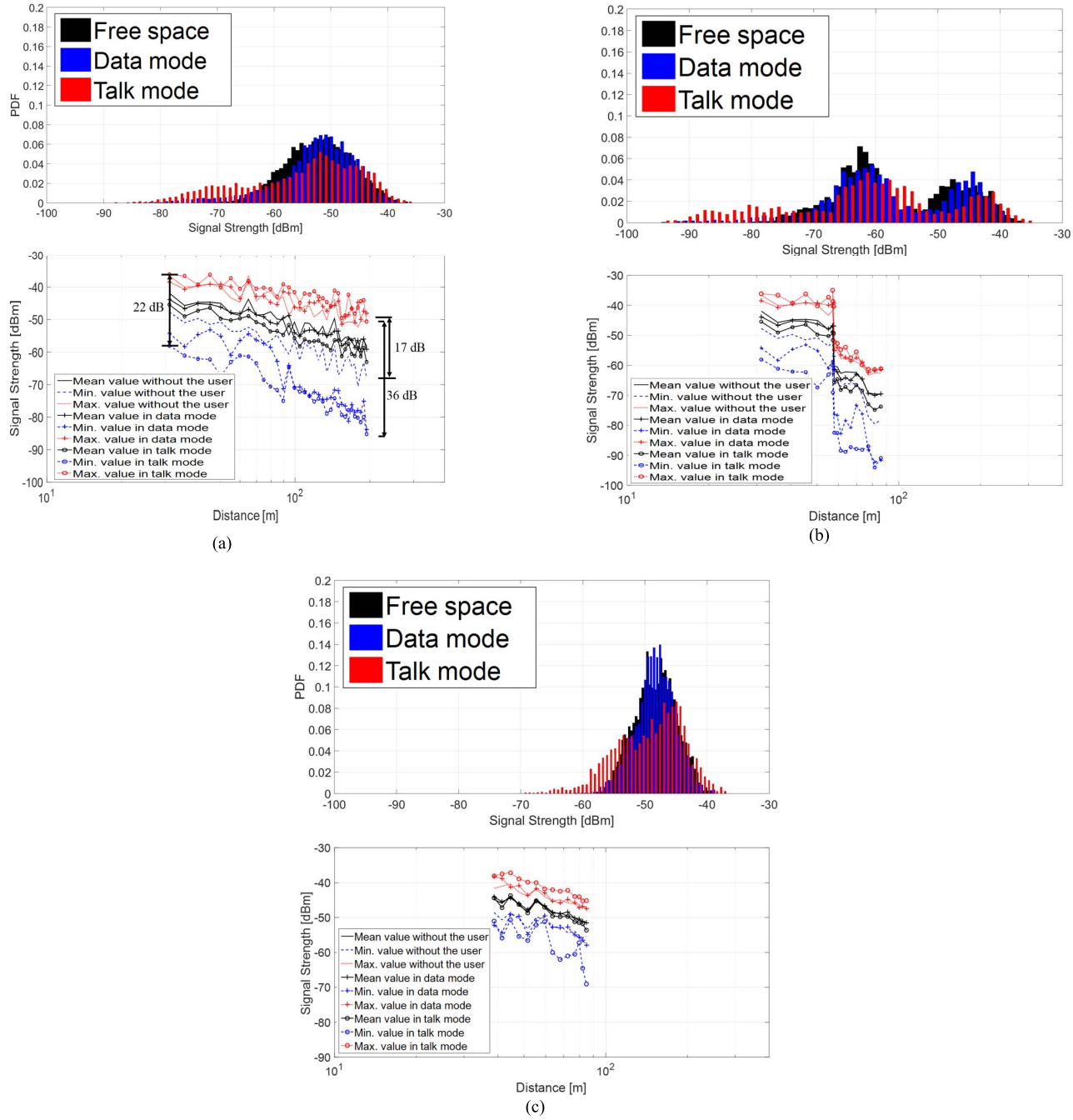


Fig. 15. PDF and variation of received signal strength in (a) urban canyon, (b) corner, and (c) parking lot environment with rotated orientation of the notch antenna integrated in the UE at 15 GHz.

The notch antenna at 15 GHz on the top of the phone mockup is chosen as an example to study. The 8×1 linear array is extended from a single embedded notch element with a half wavelength separation between each element, and the radiation patterns of each element in the array are assumed to be identical.

The dominant eigenmode beamforming algorithm is adopted in this study because it is optimal in terms of maximizing the signal-to-noise ratio [46]. This simple beamforming algorithm is sufficient here because we are only interested in evaluating the coverage capabilities of the single user case.

The beamforming is only performed on the UE side in this study, and thus a SIMO system is presented. The BS antenna is kept the same as in the previous section to highlight the effect from the UE antenna, and the 15 dB gain is still added on the received signal strength.

The performances of the single notch antenna and the 8×1 linear array are compared in the data mode and talk mode as shown in Figs. 16 and 17 (with the same orientations as shown in Fig. 9). It can be observed that a 9 dB beamforming gain is obtained from the linear array, which agrees with the theoretical value. As the beamforming gain is limited, it cannot

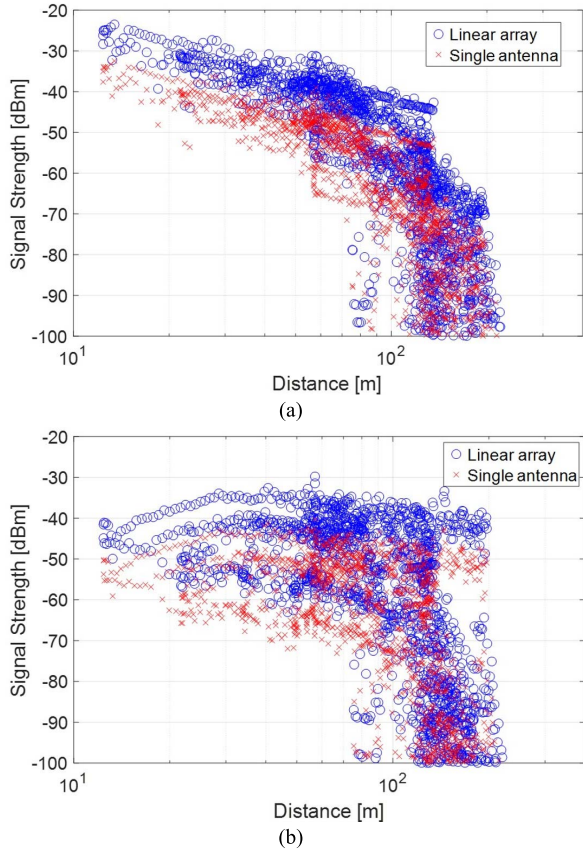


Fig. 16. Received signal strength with a single notch antenna and an 8×1 linear notch array in (a) data mode and (b) talk mode at 15 GHz.

improve the system coverage in the NLOS areas drastically because the shadowing effect from the building blockage (40–50 dB) is much higher. However, as the user body shadowing effect (20–25 dB at 15 GHz) is much smaller compared to buildings' blockage, the array scheme in the UE can mitigate the body shadowing effect to some extent if the user blocks only some propagation paths between the BS and the UE.

The received signal strength at 28 GHz with an 8×1 linear array also shows a constant 9 dB gain compared to the single antenna case, as we assume the radiation pattern of each element is identical in the simulation. Therefore, its values can be estimated from the single antenna performance in Fig. 13, and the results of 28 GHz are omitted here.

However, the linear array scheme in the UE cannot be seen as the sole solution to mitigate the user body effect on the received signal strength of UE. In practice, the space inside the UE is usually very limited, which will limit the number of antenna elements and the beamforming gain of the array. We also note that, in this paper, we have not fully explored the effect of the hands of the user. With an even larger array, the user will inevitably cover at least some of the array elements on the UE. A multiple antenna system that exploits the spatial diversity gains on the UE side and cooperative BS techniques should also be considered for future 5G cellular systems above 6 GHz. Their effect will be

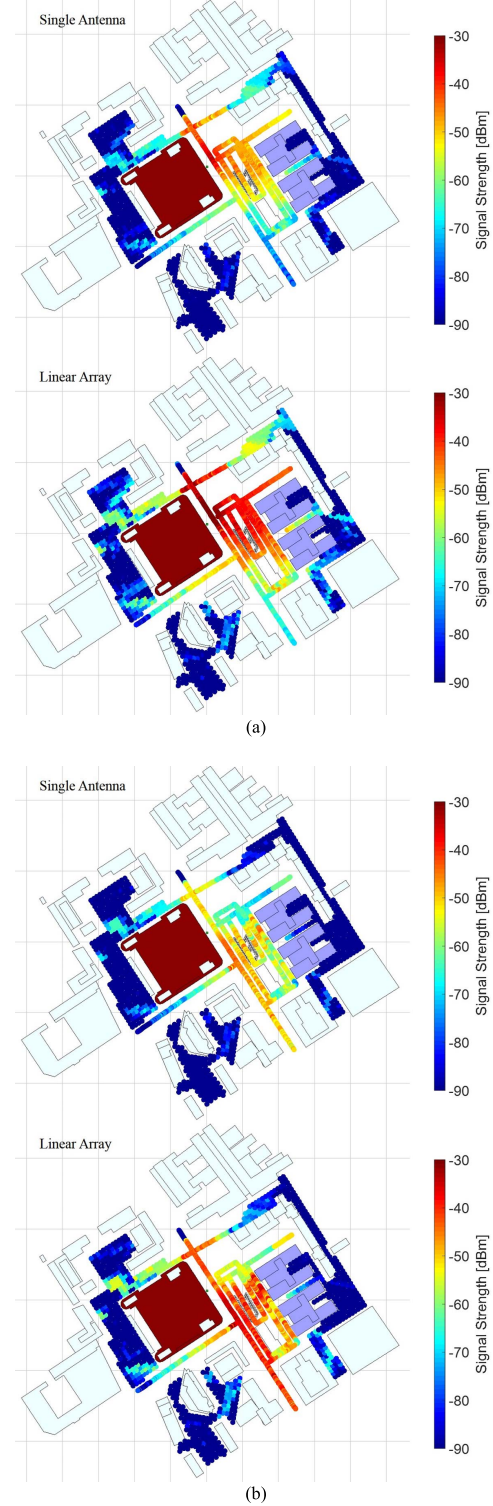


Fig. 17. Coverage overview with a single notch antenna and an 8×1 linear notch array in (a) data mode and (b) talk mode at 15 GHz.

investigated in the future studies. Furthermore, more work needs to be done on the multiuser case and optimized beamforming techniques to reduce the interference between users. Also, in the uplink, a large linear array may still be necessary to reduce its output power from UE due to human exposure limitations [47], [48].

V. CONCLUSION

In this paper, the user body effect on channel characteristics are analyzed at 15 and 28 GHz. Three antenna designs with complementary radiation patterns and polarizations are fabricated and integrated into a mobile phone prototype. The channel is modeled using 3-D ray-tracing simulations with Wireless Insite and includes effective antenna radiation patterns that are measured both without user presence and with a user in CTIA data and talk mode. At 15 GHz, the user body will cause a 25 and 30 dB shadowing loss in data mode and talk mode, respectively. Meanwhile, the shadowing loss at 28 GHz is about 5 dB higher than at 15 GHz in both user holding positions based on the measurement results. Based on the results, it can be clearly observed that the received signal quality is highly dependent on the relative positions of the UE and the user. On the other hand, the difference from different single antenna designs is minimal compared to the body impact. Therefore, the user effect is a very important factor to consider when analyzing the BS coverage, the received signal strength, or the achievable capacity in a cellular system above 6 GHz.

Moreover, the user body effect can also introduce a large fluctuation of the received signal strength when its orientation is rotated, especially when the UE is in a typical urban canyon scenario where the signal is received mainly in one direction. From the results, the absolute variation of the received signal strength due to the rotation of the UE orientation can be enlarged by 22 dB at 15 GHz and 24 dB at 28 GHz in talk mode compared to the case without user obstruction when the UE is 190 m away from BS in an urban canyon. The level of fluctuation is also related to the distance between the UE and the user's body, where a larger fluctuation will be observed if the UE is more close to the user's body. For example, the SD of the received signal strength in the urban canyon environment is increased by 2.9 dB at 15 GHz and by 3.6 dB at 28 GHz in talk mode compared to in data mode. This fluctuation may increase the outage probability of the communication system even if the UE is in the LOS region, especially when the UE is placed close to the user body, e.g., when the user is talking on the phone or when the phone is in the user's pocket. For further study, the arbitrary rotation of the UE and the user in both the horizontal and the vertical planes should be considered, and the antenna design with higher coverage efficiency may outperform others, on average [30].

By implementing an 8×1 linear array with beamforming in the UE, the received signal strength can be enhanced by 9 dB at both 15 and 28 GHz with the presence of a user, which can be used to mitigate the variation of received signal strength to some extent. However, since the beamforming gain is dependent on the number of antenna elements, this value will be limited by the space available inside the UE. Different array topologies on the UE side, cooperative BS techniques, and optimized cellular planning for cellular systems above 6 GHz should also be considered to mitigate the shadowing effect due to the user's body and buildings.

ACKNOWLEDGMENT

The authors would like to thank Dr. F. Harryson and Ericsson Research in Kista for providing measurement data. The authors would also like to thank the Microwave Vision Group for their support with performing accurate antenna measurements at 15 GHz and the partial support of AOARD.

REFERENCES

- [1] F. Rusek *et al.*, "Scaling up MIMO: Opportunities and challenges with very large arrays," *IEEE Signal Process. Mag.*, vol. 30, no. 1, pp. 40–60, Jan. 2013.
- [2] E. G. Larsson, O. Edfors, F. Tufvesson, and T. L. Marzetta, "Massive MIMO for next generation wireless systems," *IEEE Commun. Mag.*, vol. 52, no. 2, pp. 186–195, Feb. 2014.
- [3] T. S. Rappaport *et al.*, "Millimeter wave mobile communications for 5G cellular: It will work!" *IEEE Access*, vol. 1, pp. 335–349, May 2013.
- [4] *Report and Order and Further Notice of Proposed Rulemaking*, document FCC 16-89, Federal Communications Commission, Jul. 2016. [Online]. Available: <http://transition.fcc.gov/Daily%20Releases/Daily%20Business/2016/db0728/FCC-16-89A1.pdf>
- [5] E. J. Violette, R. H. Espeland, R. O. DeBolt, and F. K. Schwering, "Millimeter-wave propagation at street level in an urban environment," *IEEE Trans. Geosci. Remote Sens.*, vol. 26, no. 3, pp. 368–380, May 1988.
- [6] H. Zhao *et al.*, "28 GHz millimeter wave cellular communication measurements for reflection and penetration loss in and around buildings in New York city," in *Proc. IEEE Int. Conf. Commun. (ICC)*, Jun. 2013, pp. 5163–5167.
- [7] T. S. Rappaport, R. W. Heath, Jr., R. Daniels, and J. Murdock, *Millimeter Wave Wireless Communications*. Englewood Cliffs, NJ, USA: Prentice-Hall, 2015.
- [8] G. R. MacCartney, S. Deng, S. Sun, and T. S. Rappaport, "Millimeter-wave human blockage at 73 GHz with a simple double knife-edge diffraction model and extension for directional antennas," in *Proc. IEEE 84th Veh. Technol. Conf. (VTC-Fall)*, Sep. 2016, pp. 1–6.
- [9] C. Gustafson and F. Tufvesson, "Characterization of 60 GHz shadowing by human bodies and simple phantoms," *Radioengineering*, vol. 21, no. 4, pp. 979–984, 2012.
- [10] M. Jacob, S. Priebe, A. Maltsev, A. Lomayev, V. Erceg, and T. Kürner, "A ray tracing based stochastic human blockage model for the IEEE 802.11ad 60 GHz channel model," in *Proc. Eur. Conf. Antennas Propag. (EuCAP)*, Apr. 2011, pp. 3084–3088.
- [11] F. K. Schwering, E. J. Violette, and R. H. Espeland, "Millimeter-wave propagation in vegetation: Experiments and theory," *IEEE Trans. Geosci. Remote Sens.*, vol. 26, no. 3, pp. 355–367, May 1988.
- [12] P. F. M. Smulders, "Statistical characterization of 60 GHz indoor radio channels," *IEEE Trans. Antennas Propag.*, vol. 57, no. 10, pp. 2820–2829, Oct. 2009.
- [13] F. Villanese, N. E. Evans, and W. G. Scanlon, "Pedestrian-induced fading for indoor channels at 2.45, 5.7 and 62 GHz," in *Proc. IEEE 52nd Veh. Technol. Conf. (VTC-Fall)*, Sep. 2000, pp. 43–48.
- [14] M. Samimi *et al.*, "28 GHz angle of arrival and angle of departure analysis for outdoor cellular communications using steerable beam antennas in New York city," in *Proc. IEEE 77th Veh. Technol. Conf. (VTC-Spring)*, Jun. 2013, pp. 1–6.
- [15] Y. Azar *et al.*, "28 GHz propagation measurements for outdoor cellular communications using steerable beam antennas in New York city," in *Proc. IEEE Int. Conf. Commun. (ICC)*, Jun. 2013, pp. 5143–5147.
- [16] M. R. Akdeniz *et al.*, "Millimeter wave channel modeling and cellular capacity evaluation," *IEEE J. Sel. Areas Commun.*, vol. 32, no. 6, pp. 1164–1179, Jun. 2014.
- [17] S. Hur *et al.*, "Proposal on millimeter-wave channel modeling for 5G cellular system," *IEEE J. Sel. Topics Signal Process.*, vol. 10, no. 3, pp. 454–469, Apr. 2016.
- [18] K. Haneda *et al.*, "5G 3GPP-like channel models for outdoor urban microcellular and macrocellular environments," in *Proc. IEEE 83rd Veh. Technol. Conf. (VTC-Spring)*, May 2016, pp. 1–7.
- [19] Aalto University, BUPT, CMCC, Nokia, NTT DOCOMO, New York University, Ericsson, Qualcomm, Huawei, Samsung, Intel, University of Bristol, KT Corporation, and University of Southern California, "5G channel model for bands up to 100 GHz," Tech. Rep., Dec. 2015. [Online]. Available: <http://www.5gworkshops.com/5GCM.html>

- [20] A. F. Molisch, A. Karttunen, S. Hur, J. Park, and J. Zhang, "Spatially consistent path loss modeling for millimeter-wave channels in urban environments," in *Proc. Eur. Conf. Antennas Propag. (EuCAP)*, Apr. 2016, pp. 1–5.
- [21] A. Karttunen *et al.*, "Path loss models with distance-dependent weighted fitting and estimation of censored path loss data," *IET Microw. Antennas Propag.*, vol. 10, no. 14, pp. 1467–1474, Nov. 2016.
- [22] T. S. Rappaport *et al.*, "Wideband millimeter-wave propagation measurements and channel models for future wireless communication system design," *IEEE Trans. Commun.*, vol. 63, no. 9, pp. 3029–3056, Sep. 2015.
- [23] S. Sun *et al.*, "Investigation of prediction accuracy, sensitivity, and parameter stability of large-scale propagation path loss models for 5G wireless communications," *IEEE Trans. Veh. Technol.*, vol. 65, no. 5, pp. 2843–2860, May 2016.
- [24] M. K. Samimi and T. S. Rappaport, "3-D millimeter-wave statistical channel model for 5G wireless system design," *IEEE Trans. Microw. Theory Techn.*, vol. 64, no. 7, pp. 2207–2225, Jul. 2016.
- [25] K. Haneda, "Channel models and beamforming at millimeter-wave frequency bands," *IEICE Trans. Commun.*, vol. E98-B, no. 5, pp. 755–772, May 2015.
- [26] Technical Specification Group Radio Access Network; Study on Channel Model for Frequencies From 0.5 to 100 GHz, document TR 38.901, 3GPP, Jul. 2017.
- [27] M. Pelosi, O. Franek, M. B. Knudsen, G. F. Pedersen, and J. B. Andersen, "Antenna proximity effects for talk and data modes in mobile phones," *IEEE Antennas Propag. Mag.*, vol. 52, no. 3, pp. 15–26, Jun. 2010.
- [28] V. Plicanic, B. K. Lau, A. Derneryd, and Z. Ying, "Actual diversity performance of a multiband diversity antenna with hand and head effects," *IEEE Trans. Antennas Propag.*, vol. 57, no. 5, pp. 1547–1556, May 2009.
- [29] N. Kuster and Q. Balzano, "Energy absorption mechanism by biological bodies in the near field of dipole antennas above 300 MHz," *IEEE Trans. Veh. Technol.*, vol. 41, no. 1, pp. 17–23, Feb. 1992.
- [30] K. Zhao, J. Helander, D. Sjöberg, S. He, T. Bolin, and Z. Ying, "User body effect on phased array in user equipment for the 5G mmWave communication system," *IEEE Antennas Wireless Propag. Lett.*, vol. 16, pp. 864–867, 2017.
- [31] I. Syrtis, S. Zhang, G. Pedersen, K. Zhao, T. Bolin, and Z. Ying, "User effects on mobile terminal antennas at 28 GHz for 5G applications," *IEEE Trans. Antennas Propag.*, to be published.
- [32] M. Abouelseoud and G. Charlton, "The effect of human blockage on the performance of millimeter-wave access link for outdoor coverage," in *Proc. IEEE 77th Veh. Technol. Conf. (VTC-Spring)*, Jun. 2013, pp. 1–5.
- [33] T. Bai and R. W. Heath, Jr., "Analysis of self-body blocking effects in millimeter wave cellular networks," in *Proc. 48th Asilomar Conf. Signals Syst. Comput.*, Nov. 2014, pp. 1921–1925.
- [34] S. Y. Seidel and T. S. Rappaport, "Site-specific propagation prediction for wireless in-building personal communication system design," *IEEE Trans. Veh. Technol.*, vol. 43, no. 4, pp. 879–891, Nov. 1994.
- [35] C. Oestges, G. Hennaux, and Q. Gueuning, "Centimeter- and millimeter-wave channel modeling using ray-tracing for 5G communications," in *Proc. IEEE 82nd Veh. Technol. Conf. (VTC-Fall)*, Sep. 2015, pp. 1–5.
- [36] H. C. Nguyen *et al.*, "Evaluation of empirical ray-tracing model for an urban outdoor scenario at 73 GHz E-band," in *Proc. IEEE 80th Veh. Technol. Conf. (VTC-Fall)*, Sep. 2014, pp. 1–6.
- [37] A. Landstrom, J. van de Beek, A. Simonsson, M. Thurfjell, and P. Okvist, "Measurement-based stochastic mmwave channel modeling," in *Proc. IEEE Globecom Workshops (GC Wkshps)*, Dec. 2016, pp. 1–6.
- [38] P. Ökvist, H. Asplund, A. Simonsson, B. Halvarsson, J. Medbo, and N. Seifi, "15 GHz propagation properties assessed with 5G radio access prototype," in *Proc. 26th Annu. IEEE Int. Symp. Pers., Indoor, Mobile Radio Commun. (PIMRC)*, Sep. 2015, pp. 2220–2224.
- [39] (Dec. 3, 2015). *Spectrum Decisions at WRC-15, a Step Towards the Networked Society*. [Online]. Available: https://www.ericsson.com/news/151203-wrc-15-spectrum_244069644_c
- [40] *Wireless InSite Reference Manual, Version 2.8.0, Commercial SW User-Manual*, Remcom, Oct. 2015.
- [41] "Propagation data and prediction methods required for the design of terrestrial line-of-sight systems," Int. Telecommun. Union (ITU), Geneva, Switzerland, Tech. Rep. Rec. ITU-R P.530-16, Jul. 2015.
- [42] "Electrical characteristics of the surface of the earth," Int. Telecommun. Union (ITU), Geneva, Switzerland, Tech. Rep. Rec. ITU-R P.527-3, 1992.
- [43] *Test Plan for Wireless Device Over the-Air Performance*, CTIA Certification Program, Washington, DC, USA, Nov 2016.
- [44] F. Harrysson, J. Medbo, A. F. Molisch, A. J. Johansson, and F. Tufvesson, "Efficient experimental evaluation of a MIMO handset with user influence," *IEEE Trans. Commun.*, vol. 9, no. 2, pp. 853–863, Feb. 2010.
- [45] K. Haneda, C. Gustafson, and S. Wyne, "60 GHz spatial radio transmission: Multiplexing or beamforming?" *IEEE Trans. Antennas Propag.*, vol. 61, no. 11, pp. 5735–5743, Nov. 2013.
- [46] A. Paulraj, D. Gore, and R. Nabar, *Multiple Antenna Systems*. Cambridge, U.K.: Cambridge Univ. Press, 2003.
- [47] K. Zhao, Z. Ying, and S. He, "EMF exposure study concerning mmwave phased array in mobile devices for 5G communication," *IEEE Antennas Wireless Propag. Lett.*, vol. 15, pp. 1132–1135, 2016.
- [48] B. Thors, D. Colombi, Z. Ying, T. Bolin, and C. Törnevik, "Exposure to RF EMF from array antennas in 5G mobile communication equipment," *IEEE Access*, vol. 4, pp. 7469–7478, Nov. 2016.



Kun Zhao received the B.S. degree in communication engineering from the Beijing University of Posts and Telecommunications, Beijing, China, in 2010, and the M.S. degree in wireless systems from the KTH Royal Institute of Technology, Stockholm, Sweden, in 2012, where he is currently pursuing the Ph. D. degree with the Department of Electromagnetic Engineering.

He has been a Visiting Researcher with the Department of Electrical and Information Technology, Lund University, Lund, Sweden, and Sony AB, Sweden. His current research interests include mmWave antenna and propagation for 5G communications, MIMO antenna systems, multiple antennas-user interactions, and body centric wireless communications.

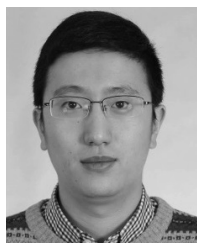


Carl Gustafson (M'16) received M.Sc. degree in electrical engineering and the Ph.D. degree in radio systems from the Department of Electrical and Information Technology, Lund University, Sweden.

He is currently a Post-Doctoral Researcher with Lund University. His current research interests include channel measurements and modeling for mmWave systems, cellular systems operating above 6 GHz, vehicular communication systems, massive MIMO, antenna array processing, statistical estimation, and electromagnetic wave propagation.



Qingbi Liao was born in Chengdu, China, in 1992. She received the bachelor's degree in communication engineering from Beijing JiaoTong University, Beijing, China, in 2014, the bachelor's degree in computer engineering from Mid Sweden University, Sundsvall, Sweden in 2014, and the master's degree in wireless communications from Lund University, Lund, Sweden. She is currently pursuing the Ph.D. degree with the Electromagnetic Engineering Department, School of Electrical Engineering, KTH Royal Institute of Technology, under the supervision of O. Quevedo-Teruel. Her Ph.D. thesis focused on wireless communications from apparatus-embedded sensors for online monitoring.



Shuai Zhang was born in Liaoning, China, in 1983. He received the B.E. degree from the University of Electronic Science and Technology of China, Chengdu, China, in 2007, and the Ph.D. degree in electromagnetic engineering from the KTH Royal Institute of Technology, Stockholm, Sweden, in 2013.

He was a Research Fellow with the KTH Royal Institute of Technology. In 2010 and 2011, he was a Visiting Researcher at Lund University, Lund, Sweden, and at Sony Mobile Communications AB, Lund, Sweden, respectively. In 2014, he joined Aalborg University, Aalborg, Denmark, where he is currently an Associate Professor. He is also an external antenna specialist at Bang & Olufsen, Struer, Denmark. His current research interests include mobile terminal mmWave antennas, biological effects, nanosatellite antennas, UWB wind turbine blade deflection sensing, MIMO antenna systems, and RFID antennas.



Zhinong Ying (SM'05) is a Principle Engineer of antenna technology in the Network research Lab within the Technology Office, Sony Mobile Communication AB, Lund, Sweden, also as a Distinguish Engineer within the whole Sony group. He joined Ericsson AB in 1995, became a Senior Specialist in 1997, and then Expert in 2003. He has also been a Guest Professor in the Joint research center of Royal institute of Technology, Sweden, and Zhejiang University, China, since 2001. He had contributed a lot of work in antenna designs and evaluation methods for the mobile industry. He has also involved in the evaluation of Bluetooth Technology which was invented by Ericsson. He has authored and co-authored over 140 papers in various journal, conference, and industry publications. He holds more than 140 patents and pending in the antennas and new generation wireless network areas. He contributed several book chapters on mobile antenna, small antenna and MIMO antennas in “mobile antenna handbook 3rd edition” edited H. Fujimoto and “handbook of antenna technologies” edited by Z. N. Chen. His current research interests include small antennas, broad and multiband antenna, multichannel antenna (MIMO) system, antenna for body area network, antenna and propagation in fifth generation mobile network including massive MIMO and mmWave, near-field, and human body effects and measurement techniques.

Mr. Ying was a member of scientific board of ACE program (Antenna Center of Excellent in European 6th frame) from 2004 to 2007. He served as TPC Co-Chairmen in International Symposium on Antenna Technology (iWAT) 2007, and served as session organizer of several international conferences including IEEE APS, and a reviewer for several academic journals. He was a recipient of the Best Invention Award at Ericsson Mobile in 1996, and the Key Performer Award at Sony Ericsson in 2002. He was nominated for President Award at Sony Ericsson for his innovative contributions in 2004. He received Distinguish Engineer title at Sony Group globally in 2013.



Thomas Bolin received the M.Sc. degree in applied physics and electrical engineering from Linköping University, Linköping, Sweden, in 1979.

From 1979 to 1983, he was an RF-Development Engineer at ITT Standard Radio & Telefon AB, Stockholm, Sweden, where he was involved in 1 kW HF PA and filter designs. From 1983 to 2011, he held a technical management position at Ericsson Mobile Communications, Lund, Sweden, where he was involved in RF and antenna product development and OTA measurement technology development for mobile handsets, and since 2011, at Sony Mobile Communications in Lund, more devoted to antenna research and standardization, frequently a 3GPP RAN 4 delegate. In late, he assisted in the development of mmWave antenna arrays and FEM integration (15–40 GHz) for 5G.

ment for mobile handsets, and since 2011, at Sony Mobile Communications in Lund, more devoted to antenna research and standardization, frequently a 3GPP RAN 4 delegate. In late, he assisted in the development of mmWave antenna arrays and FEM integration (15–40 GHz) for 5G.



Sailing He (M'92-SM'98-F'13) received the Licentiate of Technology and the Ph.D. degree in electromagnetic theory from the KTH Royal Institute of Technology, Stockholm, Sweden, in 1991 and 1992, respectively.

Since 1992, he has been with the KTH Royal Institute of Technology as an Assistant Professor, and an Associate Professor, and then a Full Professor. He is the Director for a joint research center between KTH and Zhejiang University (China). He has first-authored one monograph (Oxford University Press) and authored or co-authored about 500 papers in refereed international journals. His current research interests include applied electromagnetics, electromagnetic metamaterials, optoelectronics, microwave photonics and biomedical applications.